

Bevel Edge Termination for Vertical GaN Power Diodes

Andrew T. Binder*, Jeramy R. Dickerson, Mary H. Crawford, Greg W. Pickrell, Andrew A. Allerman, Paul Sharps, Robert J. Kaplar

Sandia National Laboratories, Albuquerque, NM 87185, USA

*abinder@sandia.gov

1 *Abstract*—Edge termination for vertical power devices39
2 presents a significant challenge, as improper termination can40
3 result in devices with a breakdown voltage significantly less than41
4 the ideal infinite-planar case. Edge termination for vertical GaN42
5 devices is particularly challenging due to limitations in ion43
6 implantation for GaN, and as such this work investigates a bevel44
7 edge termination technique that does not require implantation and45
8 has proven to be effective for Si and SiC power devices. However,46
9 due to key differences between GaN versus Si and SiC p-n47
10 junctions (specifically, a grown versus an implanted junction), this48
11 technology needs to be reevaluated for GaN. Simulation results49
12 suggest that by leveraging the effective bevel angle relationship, a49
13 10-15° physical bevel angle can yield devices with 85-90% of the49
14 ideal breakdown voltage. Results are presented for a negative49
15 bevel edge termination on an ideally 2 kV vertical GaN p-n diode.50

16 *Keywords*—vertical GaN diode; edge termination; junction51
17 termination extension; power devices52

I. INTRODUCTION

19 Optimization of breakdown in vertical power devices is55
20 often limited by field crowding at the periphery of the device.56
21 For an ideal planar device, the breakdown is limited by the peak57
22 electric field in the bulk, yielding a much higher breakdown58
23 voltage than for a device limited by a large surface electric field.59
24 To address this issue, special junction terminations around the60
25 edges of the power device can be formed so that the depletion61
26 near the surface is increased, thereby reducing field crowding.62
27 The most common edge termination structures in Si and SiC63
28 (junction termination extensions {JTEs} and guard rings) are64
29 created by selective-area doping using ion implantation.65
30 However, Mg implantation in GaN aimed at achieving66
31 selective-area p-type doping suffers from low activation67
32 efficiency and a limited effective range of implantation energy68
33 and dose [1], making this method challenging to use in GaN.69
34 power devices. An alternate junction termination method that70
35 does not require selective-area doping is the negative bevel edge.71
36 termination which has been demonstrated both in Si and SiC.72
37 power devices [2], [3]. However, epitaxially-grown p-n73
38 junctions in GaN are much more abrupt than implanted.74

75 Sandia National Laboratories is a multi-mission laboratory managed and75
76 operated by National Technology & Engineering Solutions of Sandia, LLC, a76
77 wholly owned subsidiary of Honeywell International Inc., for the U.S.77
78 Department of Energy's National Nuclear Security Administration under78
79 contract DE-NA0003525.

junctions in Si and SiC power devices [4], [5], resulting in important differences in how these regions deplete, impacting the effectiveness of a bevel termination.

In this work, a vertical GaN p-n diode is used to evaluate the performance of a negative bevel edge termination. It should be noted that this edge termination technique is not in any way limited to this particular device, but can be applied to a wide range of devices.

II. THEORETICAL BACKGROUND

A. Single-Zone/Multi-Zone JTE

The design of a single-zone or multi-zone JTE hinges on Gauss's law and the charge enclosed in the Gaussian surface (the JTE) [6], [7]. According to Gauss's law, the electric flux through any closed surface is equal to the total charge inside divided by the permittivity as shown in Eq. 1:

$$\phi = E \cdot A = \frac{\sigma \cdot A}{\epsilon_r \cdot \epsilon_0} \quad (1)$$

where ϕ is the electric flux, σ is the charge per unit area, ϵ is the permittivity, A is the area of the Gaussian surface, and E is the electric field.

In this manner, the charge inside the JTE acts as a sink for the electric field in a power device at breakdown, causing the field lines to terminate into the JTE and not crowd at the periphery of the device. Premature breakdown occurs in unterminated devices when field crowding at the periphery of the device causes the surface E-field to exceed the bulk E-field by a significant margin. In properly terminated devices, at breakdown the E-field at the surface will be equal to the E-field in the bulk thereby maximizing the breakdown voltage of the device. An ideal termination is obtained when the charge in the JTE is designed to sink the critical electric field (E_{crit}).

The disadvantage of a single-zone JTE (SZ-JTE) is that the JTE efficiency (the ratio of the breakdown voltage in a terminated device to the breakdown voltage of an ideal one-dimensional device) is very sensitive to changes in total charge within the Gaussian surface, and therefore sensitive to the thickness and doping density of the JTE [8], [9]. One method to reduce this sensitivity to process variation is to design a multi-zone JTE (MZ-JTE) which employs several JTEs each with a

unique total JTE charge [9]. However, each additional zone requires additional fabrication steps, further complicating the process. In addition, both the SZ-JTE and MZ-JTE suffer from adverse effects of surface charge that strongly depend on passivation, which needs careful consideration when designing for the optimal total JTE charge. Surface charge resulting from passivation can effectively reduce voltage-blocking capability by 25-50% depending on the net interface state density [10].

87 B. Bevel Edge Termination

88 The analog approach to a step change in charge across
89 multiple regions (MZ-JTE) is to create a bevel with a continuum
90 of charge. With a bevel, the charge in the Gaussian surface is
91 not a discrete value that can be hit or missed due to process
92 variation, but rather is a continuous range which is less sensitive
93 to changes in total JTE charge. In direct contrast to the SZ/MZ-
94 JTE, the effectiveness of the bevel edge termination is also
95 insensitive to surface charge, due to the continuum of charge in
96 the bevel.

97 The design for a bevel edge termination is primarily based
98 on two factors: the ratio of the depletion depth into the JTE to
99 the depletion into the drift region, and the angle of the bevel. A
100 negative bevel with a small bevel angle can be used to reduce
101 the peak surface electric field by increasing the depletion width
102 on the surface relative to the depletion width in the bulk as
103 shown in Fig. 1. The increased surface depletion in turn reduces
104 the E-field at the surface, given that a constant voltage across a
105 greater depletion width yields a smaller E-field ($E = dv/dx$). When
106 the bevel angle is sufficiently small the E-field at the
107 surface will be equal to or less than the E-field in the bulk,
108 yielding near-ideal breakdown performance in the terminated
109 device.

110 C. Effective Bevel Angle

111 For a beveled device, the edge termination becomes more
112 effective for the same bevel angle when the depletion depth into
113 the bevel (x_p) increases (see Fig. 1) [11], [12]. This relationship
114 can be expressed in terms of an effective bevel angle. 136

115 One fundamental difference between junctions in GaN
116 versus junctions in SiC or Si devices is that generally GaN
117 junctions are grown and are therefore much more abrupt than
118 SiC junctions, which are implanted or diffused. This
119 fundamental difference has a significant impact on the effective
120 bevel equation. As Adler *et al.* [11] demonstrate in their early
121 paper, for a diffused junction the effective bevel angle is
122 function of the ratio of the depletions widths squared (Eq. 2),
123 but for an abrupt junction it is simply the ratio of the depletioh44
124 widths (Eq. 3): 145

$$126 \quad \text{Diffused Junction: } \theta_{eff} = 0.04 \cdot \theta_{act} \cdot \left(\frac{x_{DB}^-}{x_{DB}^+} \right)^2 \quad (2) \quad 146$$

$$128 \quad \text{Abrupt Junction: } \theta_{eff} = 0.04 \cdot \theta_{act} \cdot \left(\frac{x_{DB}^-}{x_{DB}^+} \right) \quad (3) \quad 149$$

130 where θ_{act} is the physical bevel angle, x_{DB}^- is the depletion width
131 into the lightly-doped side at breakdown (i.e. x_n), and x_{DB}^+ is the
153 154

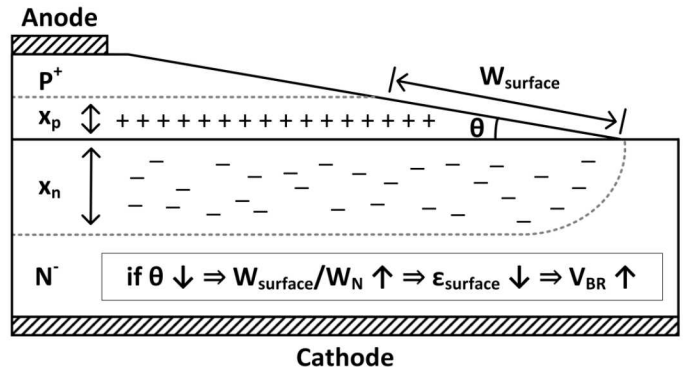


Fig. 1. Representation of fundamental theory for a negative bevel edge termination.

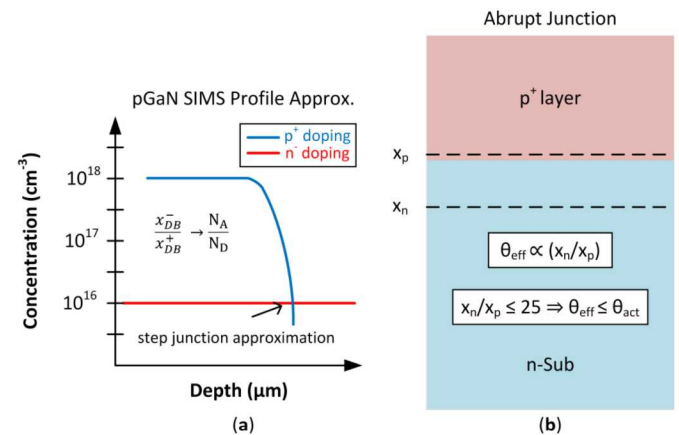


Fig. 2. Simplified representation of (a) the doping profile for an epitaxially grown p-n junction in GaN, and (b) an example of an abrupt junction and the associated bevel angle relationships.

depletion width into the heavily-doped side at breakdown (i.e. x_p).

Accordingly, an abrupt junction profile can be more easily leveraged to produce an effective bevel angle that is smaller than the physical bevel angle, making GaN an inherently better candidate for a bevel edge termination compared to Si or SiC. For an epitaxially-grown GaN p-n junction the doping profile approximates a step junction as depicted in Fig. 2(a). In the case of a step junction the ratio of the depletion widths is equal to the inverse of the ratio of the doping density in the two regions (Eq. 4).

$$126 \quad \frac{x_n}{x_p} = \frac{N_A}{N_D} \quad (4)$$

The effective bevel angle equation acts as a normalization factor to evaluate the impact of bevel angle considering variation in doping on either side of the junction. In practice, however, it is also possible to use this equation to leverage the physical bevel angle by manipulating the doping such that the effective bevel angle is smaller than the physical bevel angle. This results in high breakdown performance but with a larger bevel angle, thus increasing the manufacturability of such a structure. The effective bevel angle will be smaller than the

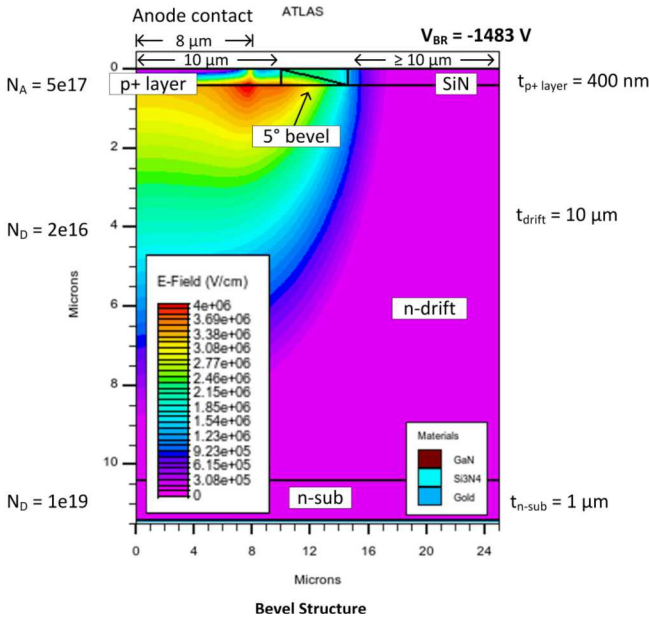


Fig. 3. Baseline simulation structure used to evaluate the negative bevel edge termination.

TABLE I
SIMULATION PARAMETERS AND VALUES

Symbol	Quantity	Value
E_g	GaN Bandgap	3.44 eV
E_{crit}	Critical Electric Field	4 MV/cm
ϵ_s	Relative Permittivity	9.7
T	Temperature	300 K
μ_p	Hole Mobility	11 cm ² /Vs
μ_n	Electron Mobility	1200 cm ² /Vs

155 physical angle when $x_n/x_p \leq 25$ resulting from the relationship⁸⁸
 156 shown in Eq. 3. This can be achieved by increasing the⁸⁹
 157 thickness of the p-GaN layer and lowering the doping⁹⁰
 158 increase the depletion depth into the p-layer. The study of⁹¹
 159 effective bevel design for a vertical GaN device is presented⁹²
 160 in the following sections.

III. DEVICE DESIGN AND SIMULATION MODEL

161 To evaluate the impact of a bevel edge termination on⁹³
 162 vertical GaN power diode, we evaluate breakdown performance⁹⁴
 163 focusing specifically on the influence of bevel angle, p-GaN⁹⁵
 164 doping concentration, and p-GaN thickness. These results are⁹⁶
 165 compared to the ideal one-dimensional device breakdown⁹⁷
 166 yield a performance figure that is the ratio of the breakdown⁹⁸
 167 voltage in the terminated device to the ideal breakdown voltage⁹⁹
 168 ($V_B(\text{beveled})/V_B(\text{planar})$), also referred to as the JTE efficiency.¹⁰⁰

169 The device under study is nominally a 2 kV p-n junction¹⁰¹
 170 power diode with a drift thickness and doping of 10 μm and¹⁰²
 171 $\times 10^{16} \text{ cm}^{-3}$ respectively. The baseline simulation structure used¹⁰³
 172 for evaluation is shown in Fig. 3 with all listed parameters held¹⁰⁴
 173 constant with the exception of bevel angle, p-layer doping, and¹⁰⁵
 174 p-layer thickness.

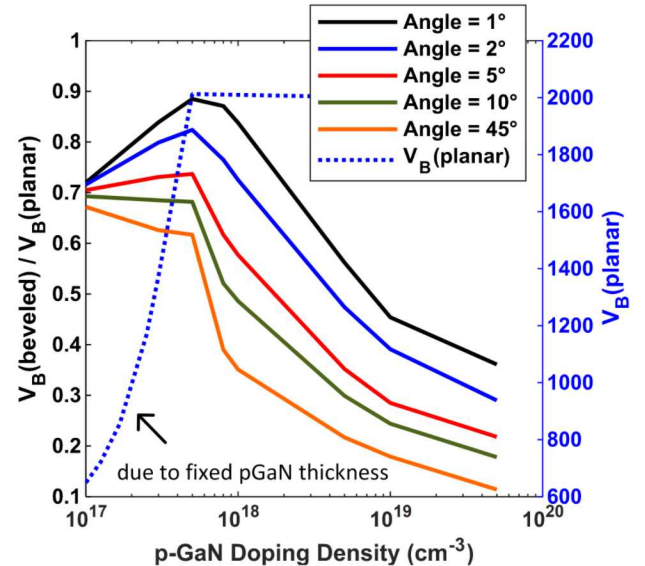


Fig. 4. Normalized breakdown voltage versus p-GaN doping density for varying bevel angles at $t_{p\text{GaN}} = 400 \text{ nm}$ (left y-axis), and ideal breakdown voltage versus p-GaN doping (right y-axis).

Device simulations were performed with Silvaco TCAD [13] to determine the reverse-bias avalanche breakdown voltage. Breakdown for the simulation is defined as the point at which the reverse-bias current density reaches 10 mA/mm², indicating the onset of avalanche. Impact ionization coefficients were specified such that at a drift doping of $2 \times 10^{16} \text{ cm}^{-3}$ the critical electric field (E_{crit}) is 4 MV/cm [14] which determines the point at which breakdown occurs. Further simulation parameters are given in Table 1 and were developed previously in [15] and [16] for similar vertical-GaN-based simulation work.

IV. RESULTS AND DISCUSSION

For a fixed drift layer design (fixed drift layer thickness and doping) the design of the bevel is dependent on three parameters: bevel p-layer thickness, p-layer doping, and bevel angle. The design considerations for bevel thickness and p-layer doping should be linked, with the desired design outcome being to maximize the depletion depth of the bevel, which serves to leverage the effective bevel angle relationship. By increasing the depletion depth into the bevel, the physical bevel angle can be increased while still yielding the same breakdown performance. This is very desirable considering that shallow (< 10°) bevel angles can not only consume a considerable amount of wafer area but are difficult to manufacture.

Normalized breakdown voltage versus p-layer doping is shown in Fig. 4 for a fixed p-GaN thickness of 400 nm. In addition, the breakdown voltage for the ideal device is shown on the right axis for comparison. Notice that for $N_A \leq 5 \times 10^{17} \text{ cm}^{-3}$ the ideal breakdown voltage drops sharply. This is an example of what happens when the p-region under the anode contact fully depletes and can be corrected simply by increasing the p-GaN thickness or doping so that the layer does not fully deplete. From this figure it is seen that at $N_A = 5 \times 10^{17} \text{ cm}^{-3}$ a bevel angle of 1° approaches 90% of the ideal breakdown voltage, but a 5° bevel is only 75% ideal. It is important to note

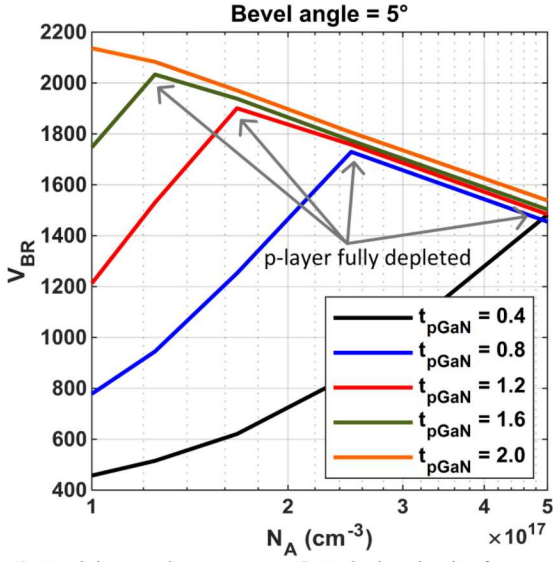


Fig. 6. Breakdown voltage versus p-GaN doping density for varying p-GaN thickness (in μm).

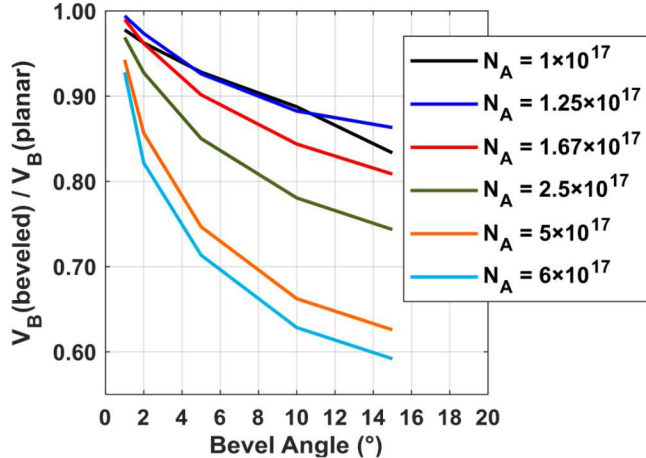


Fig. 5. Normalized breakdown voltage versus bevel angle for $t_{p\text{GaN}} = 2 \mu\text{m}$.

211 that for these doping levels, the effective bevel angle is equal to
 212 the physical angle, with the drift doping set to $2 \times 10^{16} \text{ cm}^{-3}$ and
 213 the p-layer doping at $5 \times 10^{17} \text{ cm}^{-3}$ (see Eq. 3). This means that
 214 the effective bevel angle relationship is completely
 215 unleveraged.

216 To leverage the effective bevel angle relationship, the p-
 217 layer doping should be reduced below $5 \times 10^{17} \text{ cm}^{-3}$ for the
 218 given drift doping. Since the depletion depth into the p-layer is
 219 directly proportional to the doping concentration, reducing the
 220 doping by a factor of five requires a p-layer that is five times
 221 thicker. As mentioned previously, while a single-zone JTE is
 222 very sensitive to both doping density and thickness of the JTE,
 223 a bevel edge termination does not require precise control of
 224 these variables to achieve good breakdown performance. This
 225 is highlighted in Fig. 5 which shows similar expected
 226 breakdown voltage as the p-layer thickness is varied, and an
 227 overall increase in breakdown voltage as the doping is reduced
 228 so long as the doping is not reduced to the point that the layer
 229 under the anode contact fully depletes.

230 Given that a much thicker p-layer is needed to accommodate
 231 doping down to $1 \times 10^{17} \text{ cm}^{-3}$, Fig. 6 shows the impact on

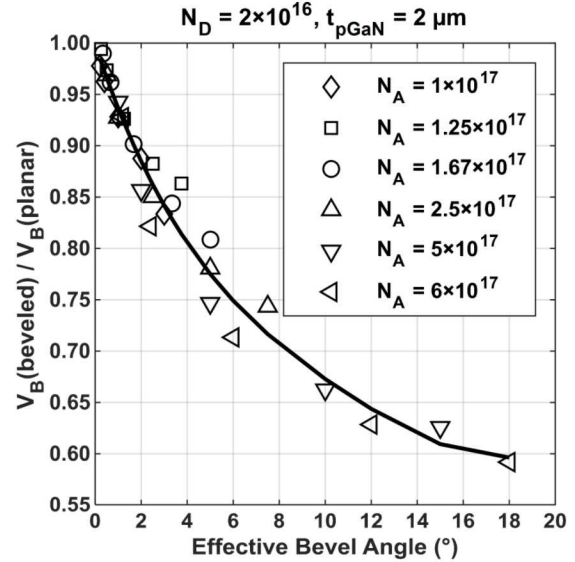


Fig. 7. Effective bevel angle plot normalizes the bevel angle to account for variations in doping.

32 breakdown performance of bevel angles less than 15° given
 33 $t_{p\text{GaN}} = 2 \mu\text{m}$. Note that as the bevel approaches the fully
 34 depleted scenario (at $1 \times 10^{17} \text{ cm}^{-3}$) the increase in breakdown
 35 performance begins to saturate, with results for $1-1.25 \times 10^{17}$
 36 cm^{-3} yielding similar breakdown performance. However, at this
 37 doping level ($1-1.25 \times 10^{17} \text{ cm}^{-3}$) it is possible to achieve nearly
 38 90% of the ideal breakdown voltage for a bevel angle of 10° .
 39 This is a considerable improvement over the 1° bevel angle
 40 necessary to approach 90% ideality at $N_A = 5 \times 10^{17} \text{ cm}^{-3}$.

41 The data from Fig. 6 can be reduced to a single function by
 42 normalizing the data using the effective bevel relationship in
 43 Eq. 3. This normalization accounts for variation in doping and
 44 demonstrates a very good fit, showcasing the accuracy of the
 45 analytical equation for an abrupt junction (Eq. 3). This
 46 normalized data is presented in Fig. 7 demonstrating that for an
 47 effective bevel angle of less than 1° it is possible to reach near
 48 100% ideality for breakdown performance. The symbols in Fig.
 49 7 represent the discrete datapoints from the simulations
 50 represented in Fig. 6 normalized using Eq. 3.

51 To obtain such a high level of breakdown performance, it is
 52 necessary to significantly leverage the effective bevel angle
 53 equation by using a very low-doped and consequently very
 54 thick p-layer, or by fabricating very shallow bevel angles.
 55 Fabricating a very thick p-layer with low doping is generally
 56 undesirable due to the negative impact on forward resistance
 57 (R_{on}). However, by employing a moderate approach with
 58 respect to p-layer doping and thickness, it is possible to take
 59 advantage of the effective bevel relationship without
 60 significantly increasing R_{on} .

V. CONCLUSION

61 The bevel edge termination is fundamentally a very
 62 attractive approach to realizing the full breakdown performance
 63 for a vertical power device. In contrast to a single/multi-zone
 64 JTE, the bevel design is robust to changes in p-layer doping and
 65 thickness. While surface charge from passivation can kill a MZ-
 66 JTE due to the discrete total charge in each zone, the bevel's

268 continuum of charge makes it more tolerant of surface charge³⁰¹
 269 However, from a fabrication standpoint there are significant³⁰²
 270 challenges to overcome to produce such a shallow (10-15°)³⁰³
 271 bevel angle. In contrast, a multi-zone JTE is relatively³⁰⁴
 272 straightforward to process, although adding more zones come³⁰⁵
 273 at the cost of higher complexity.³⁰⁶ 307

274 The simulation results presented in this work demonstrate³⁰⁸
 275 the capability of a negative bevel edge termination to achieve³⁰⁹
 276 near 90% breakdown ideality for a 10-15° physical bevel angle.³¹⁰ 311

277 This is achieved by leveraging the effective bevel angle³¹²
 278 relationship. Increasing the depletion depth into the bevel³¹³
 279 compared to the drift depletion yields higher breakdown³¹⁴
 280 performance for the same given bevel angle. In this way,³¹⁵
 281 leveraging the effective bevel angle relationship can serve³¹⁶
 282 increase the manufacturability of the bevel by relaxing the³¹⁷
 283 bevel angle requirement necessary for high breakdown³¹⁸
 284 performance. Not only does a 10° bevel angle take up less³¹⁹
 285 wafer real estate than a 1° bevel, but it is also much more³²⁰
 286 feasible to fabricate.³²¹ 322

287 Doping profiles for epitaxially-grown GaN p-n junctions are³²³
 288 much more abrupt compared to implanted junctions³²⁴
 289 characteristic of SiC power devices. As demonstrated by the³²⁵
 290 analytical equations, the effective bevel angle relationship³²⁶
 291 be more easily leveraged with an abrupt junction (GaN) than³²⁷
 292 with an implanted junction (SiC). This gives the bevel edge³²⁸
 293 termination even more significance for GaN based power³²⁹
 294 devices.³³⁰ 331

295 REFERENCES 332
 296 [1] M. J. Tadjer *et al.*, "Selective p-type Doping of GaN:Si by Mg Implantation and Multicycle Rapid Thermal Annealing," *ECS J. Solid State Sci. Technol.*, vol. 5, no. 2, pp. P124–P127, Dec. 2016. 333
 297 [2] W. Sung, A. Q. Huang, and B. J. Baliga, "Bevel junction termination extension - A new edge termination technique for 4H-SiC high-voltage³³⁴
 298 devices," *IEEE Electron Device Lett.*, vol. 36, no. 6, pp. 594–596, 2015. 335
 299 [3] H. K. Sung *et al.*, "Vertical and bevel-structured SiC etching techniques incorporating different gas mixture plasmas for various microelectronic applications," *Sci. Rep.*, vol. 7, no. 1, 2017. 336
 300 [4] H. Ohta *et al.*, "Vertical GaN p-n Junction Diodes With High Breakdown Voltages Over 4 kV," *IEEE ELECTRON DEVICE Lett.*, vol. 36, no. 11, 2015. 337
 301 [5] I. Stricklin *et al.*, "Investigation of interfacial impurities in m-plane GaN regrown p-n junctions for high-power vertical electronic devices," in *Wide Bandgap Power and Energy Devices and Applications III*, 2018, vol. 10754, p. 1. 338
 302 [6] T. Kimoto and J. A. Cooper, *Fundamentals of Silicon Carbide Technology*. Wiley, 2014. 339
 303 [7] B. J. Baliga, *Fundamentals of power semiconductor devices*. Boston, MA: Springer US, 2008. 340
 304 [8] X. Wang and J. A. Cooper, "Optimization of JTE Edge Terminations for 10 kV Power Devices in 4H-SiC," *Mater. Sci. Forum*, vol. 457–460, pp. 1257–1262, 2009. 341
 305 [9] W. Tantraporn and V. A. K. Temple, "Multiple-Zone Single-Mask Junction Termination Extension-A High-Yield Near-Ideal Breakdown Voltage technology," 1987. 342
 306 [10] H. Yilmaz, "Optimization and Surface Charge Sensitivity of High-Voltage Blocking Structures with Shallow Junctions," 1991. 343
 307 [11] M. S. Adler and V. A. K. Temple, "A General Method for Predicting the Avalanche Breakdown Voltage of Negative Bevelled Devices," 1976. 344
 308 [12] M. S. Adler and V. A. K. Temple, "Maximum surface and bulk electric fields at breakdown for planar and beveled devices," 1978. 345
 309 [13] "Silvaco TCAD." [Online]. Available: <https://www.silvaco.com/products/tead.html>. [Accessed: 21-Aug-2019]. 346
 310 [14] A. Armstrong *et al.*, "High voltage and high current density vertical GaN power diodes," 2016. 347
 311 [15] J. R. Dickerson *et al.*, "Vertical GaN Power Diodes With a Bilayer Edge Termination," *IEEE Trans. Electron Devices*, vol. 63, no. 1, p. 419, 2016. 348
 312 [16] J. J. Wierer, J. R. Dickerson, A. A. Allerman, A. M. Armstrong, M. H. Crawford, and R. J. Kaplar, "Simulations of Junction Termination Extensions in Vertical GaN Power Diodes," *IEEE Trans. Electron Devices*, vol. 64, no. 5, pp. 2291–2297, 2017. 349